Published by :
https://www.ijert.org/
An International Peer-Reviewed Journal

International Journal of Engineering Research & Technology (IJERT)
ISSN: 2278-0181
Vol. 14, Issue 09, RTMSE-2026

Combined Influence of Surface Roughness and Residual Stress on the Rotating Bending Fatigue Life of Case-Carburized EN353 Low Alloy Steel

Kumar Sushil
Department of Mechanical Engineering
Punjabi University
Patiala - 147002, Punjab, India
sushilgargiitd@gmail.com

Dr. Balraj Singh Saini
Department of Mechanical Engineering
Punjabi University
Patiala - 147002, Punjab, India

Abstract - This study reports on how surface finish and near-surface residual stress jointly govern the rotating bending fatigue response of case-carburized EN353 low alloy steel, a material widely used in automotive shafts, spindles and gear components. Specimens were carburized, hardened and finished to three distinct surface conditions and tested in fully reversed rotating bending (R = -1). Surface topography was captured with a white-light interferometric profilometer and condensed into an effective fatigue notch factor (EFNF); residual stresses, measured by X-ray diffraction, were converted into a residual stress influence factor (RSIF) through superposition on the mean bending stress. Fractographic inspection followed testing to relate crack initiation behaviour to surface condition. Fatigue life fell steeply as the surface roughened, while the compressive residual stresses left behind by carburizing extended life substantially at the same nominal stress amplitude. A combined EFNF-RSIF expression, used to adjust the applied stress amplitude before it is compared with a baseline S-N curve, reproduced the measured lives to within a factor of 1.07 to 1.22 across all three surface conditions, supporting its use as a practical, non-destructive-compatible tool for assessing rotating bending fatigue in case-hardened power-transmission components.

Keywords - Rotating bending fatigue; case carburizing; EN353 steel; surface roughness; residual stress; effective fatigue notch factor; fatigue life prediction

I. INTRODUCTION

Shafts, axles and gear spindles inside gearboxes, driveshafts and wheel-hub assemblies rarely see a steady load; instead they turn under a bending moment that reverses at every revolution, so any given point on the surface passes from tension to compression and back once per cycle. Because these parts sit at the heart of the power path, a fatigue failure in one of them is rarely a minor event - it can bring down the whole driveline and, in a vehicle or a piece of rotating machinery, put people at risk [1].

Case carburizing remains one of the principal ways of hardening the surface of such components. The process diffuses carbon into a shallow surface layer, and subsequent quench-and-temper treatment turns that layer into hard martensite while the interior stays comparatively tough. The resulting hard case-over-tough-core structure is what gives carburized parts their good wear and bending fatigue resistance [2], [3]. That benefit is not unconditional, however: how the part was machined and finished before or after carburizing, and the resulting pattern of residual stress left in the case, both have a strong say in how long the component actually lasts in service.

Roughness works against fatigue life in two related ways - the peaks and valleys on a machined surface act as small stress raisers that give cracks somewhere to start, and they also change the effective stress the material actually feels at the surface. Hardened, high-strength steels are particularly sensitive to this because they have little ductility to blunt a sharp notch. Traditional notch-factor methods, built around idealised single-groove geometries, do not capture the messiness of a real machined surface. The effective fatigue notch factor (EFNF) concept gets around this by working directly from measured three-dimensional surface topography, which makes it a more realistic descriptor of the roughness-fatigue link [4], [5].

Residual stresses are the self-balancing internal stresses that remain in a part once external load has been removed. In a carburized and quenched component, the volume change that comes with martensitic transformation in the case, combined with the way the case and core cool at different rates, leaves behind compressive stress in the surface layer. Because this compressive field partly cancels the tensile part of the applied bending stress, it slows both the start and the early growth of fatigue cracks [6]. Tensile residual stress - which can appear after aggressive grinding or an improperly controlled quench - has the opposite, damaging effect.

A great deal has been published on carburized-steel fatigue, and separately on the roles of roughness and of residual stress, but a single validated model that brings surface roughness and residual stress together for rotating bending fatigue prediction is still hard to find. The present work tries to close that gap: an EFNF derived from measured 3-D surface topography is combined with an RSIF obtained by superposing the measured residual stress on the mean bending stress, and the combined framework is checked against rotating bending fatigue tests on carburized EN353 steel at R = -1.

II. BACKGROUND

A. Fatigue of Case-Hardened Steels

The fatigue response of case-hardened steels has been studied since the mid-twentieth century. Early work by Parrish [9] catalogued the microstructural and mechanical changes brought about by carburizing and heat treatment, and later studies by Krauss [10] and Bensely et al. [11] tied retained austenite content, carbide distribution and case depth to how cracks nucleate and grow. For bending fatigue specifically, Asi et al. [12] showed that case depth and surface hardness are the main levers governing fatigue strength of carburized gear steels under cyclic bending.

B. Surface Roughness and Fatigue

Neuber [13] provided the original theoretical basis for treating roughness as a notch effect. Murakami and Endo [14] later showed that surface defects can be characterised through the square root of their projected area, underlining just how notch-sensitive high-strength steels are to surface damage. Novovic et al. [5] found that areal (3-D) roughness parameters such as Sq and Ssk describe the fatigue-relevant features of a surface far better than a single Ra value can, and Arola and Ramulu [15] built an effective stress-concentration model directly from measured valley geometry and spacing.

C. Residual Stress and Fatigue

That compressive residual stress helps rotating bending fatigue life is well established [16]. The Goodman and modified-Goodman relationships offer a simple way of folding a mean-stress-like residual stress term into a fatigue life estimate [17]. Zhuang and Halford [18] pointed out that residual stress is not necessarily stable under cyclic loading and can relax over the life of the component, which matters for long-life predictions. Torres and Voorwald [19], working on shot-peened AISI 4340 steel, showed that roughness and residual stress need to be considered together, not separately, if the fatigue life estimate is to be trustworthy.

D. EN353 Steel

EN353, equivalent to AISI 8620 / DIN 21NiCrMo2, is a Ni-Cr-Mo case-hardening steel commonly specified for automotive transmission and powertrain parts because it hardens well, carburizes cleanly and keeps good core toughness. Its heat-treatment response and mechanical properties have been documented before [20], [21], but studies that look at combined surface-integrity effects on its rotating bending fatigue behaviour are still comparatively rare.

III. MATERIALS AND EXPERIMENTAL PROCEDURE

A. Material

Normalized EN353 low alloy steel bar stock conforming to IS:4432 was used throughout. Table I lists the nominal composition range together with the composition actually measured by optical emission spectroscopy on the test material.

TABLE I. CHEMICAL COMPOSITION OF EN353 STEEL (WT.%)

Element	Nominal Range	Measured
C	0.17 - 0.23	0.20
Si	0.15 - 0.35	0.27
Mn	0.60 - 0.95	0.78
Cr	0.90 - 1.20	1.05
Ni	1.50 - 2.00	1.74
Mo	0.15 - 0.25	0.21
S (max)	0.040	0.018
P (max)	0.040	0.015
Fe	Balance	Balance

(Source: optical emission spectroscopy, present study)

B. Specimen Preparation

Rotating-bending specimens were machined from the normalized bar stock following ISO 1183 practice for force-controlled fatigue testing (Fig. 1). Three surface finishes were produced on otherwise identical specimens: Group A by precision grinding (target Sa ≈ 0.19 µm), Group B by fine turning with a finishing pass (target Sa ≈ 0.76 µm), and Group C by conventional turning only (target Sa ≈ 1.98 µm).

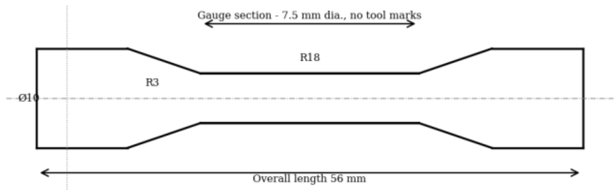

Fig. 1. Schematic of the rotating-bending fatigue specimen (gauge diameter 7.5 mm, overall length 56 mm).

C. Carburizing and Heat Treatment

All specimens were case-carburized together in a sealed-quench gas furnace using a propane-enriched endothermic atmosphere, then direct-quenched and tempered; the process parameters are summarised in Table II. The target effective case depth (to the 550 HV isopleth) was 0.8 - 1.0 mm.

TABLE II. CARBURIZING AND HEAT TREATMENT PARAMETERS

Parameter	Value / Condition
Carburizing temperature	920 °C
Atmosphere	Endothermic + propane
Carbon potential - boost	1.10% C
Carbon potential - diffuse	0.80% C
Total cycle time	6.5 h
Quench medium	Oil at 60 °C
Tempering	170 °C / 2 h
Target case depth	0.8 - 1.0 mm (550 HV)
Core hardness achieved	32 - 38 HRC
Surface hardness achieved	58 - 62 HRC

The microhardness-depth trace in Fig. 2 shows the expected gradient from a hard martensitic case (730 - 780 HV at the surface) down to a softer core (320 - 380 HV), with the 550 HV criterion locating the effective case boundary between about 0.82 and 0.97 mm - within the design target for all three groups.

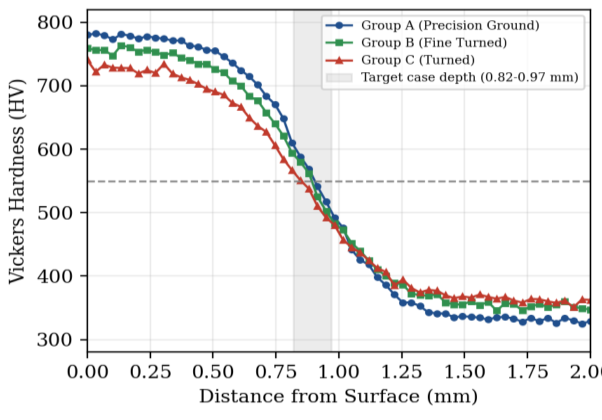

Fig. 2. Microhardness-depth traces for the three specimen groups; the dashed line marks the 550 HV case-depth criterion.

International Journal of Engineering Research & Technology (IJERT)
ISSN: 2278-0181
Vol. 14, Issue 09, RTMSE-2026

D. Surface Topography Measurement

Areal surface topography (1.5 mm × 1.5 mm fields, three positions per specimen around the gauge circumference, averaged) was acquired with a white-light interferometric profilometer (Zygo NewView 9000) before fatigue testing and reduced with MountainsMap® software following ISO 25178. Representative traces for the three groups appear in Fig. 3, and the areal parameters that feed the EFNF calculation are listed in Table III.

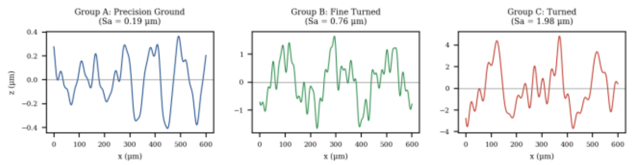

Fig. 3. Representative surface-profile traces (600 µm scan length) for Groups A, B and C.

TABLE III. MEASURED AREAL SURFACE PARAMETERS (MEAN ± SD, N = 5)

Parameter	Grp A	Grp B	Grp C
Sa (µm)	0.19±0.02	0.76±0.06	1.98±0.14
Sq (µm)	0.24±0.03	0.97±0.08	2.51±0.18
Sz (µm)	2.1±0.3	7.8±0.6	21.4±2.1
Ssk	-0.31±0.05	-0.18±0.04	0.12±0.07
Sku	3.2±0.2	3.5±0.3	3.8±0.4
Sdq (rad)	0.08±0.01	0.22±0.02	0.48±0.04
Sdr (%)	0.31±0.05	2.37±0.18	10.60±0.90

E. Residual Stress Measurement

Surface and sub-surface residual stresses were measured by X-ray diffraction (Proto LXRD, Cr-Kα radiation, $\lambda = 0.229$ nm) on the {211} plane ($2\theta \approx 156°$) using the $\sin^2\psi$ method ($\psi = 0°, \pm15°, \pm30°, \pm45°$), with X-ray elastic constants $S_1 = -1.25\times10^{-6}$ MPa^{-1} and $½S_2 = 5.81\times10^{-6}$ MPa^{-1}. Depth profiles (Fig. 4) were obtained by electrochemical layer removal on selected specimens; surface values for all specimens are summarised in Table IV.

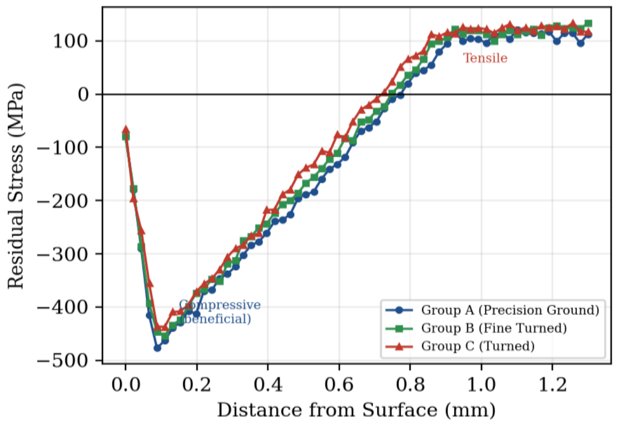

Fig. 4. Residual-stress depth profiles (post heat treatment). Peak compressive stress occurs 0.05-0.10 mm below the surface.

TABLE IV. SURFACE RESIDUAL STRESS BY GROUP (MPA)

Group	After Machining	After Carb.+HT	After Finishing
A	-85±12	-420±28	-380±22
B	+45±18	-395±31	-395±31
C	+120±25	-360±35	-360±35

Negative = compressive; positive = tensile. Final finishing on Group A partly relaxed the grinding-induced compressive layer.

F. Rotating Bending Fatigue Testing

Fatigue tests were run on a four-point rotating bending machine at a constant 3000 rpm (50 Hz), load-controlled, $R = -1$, in laboratory air (23±2 °C, 45±10% RH). Stress amplitudes from 400 to 900 MPa were covered, with tests stopped at fracture or at a run-out of 10^7 cycles. At least two specimens per stress level and five stress levels per group were tested. Because every surface fibre sees a full tension-compression reversal each revolution, this configuration reproduces the loading a shaft experiences in service.

G. Fractography

Fracture surfaces were cleaned ultrasonically in acetone and examined with a Zeiss Axio optical microscope (50× - 500×) to locate crack-initiation sites, beach marks and the final fast-fracture zone, and to relate these features back to the roughness and residual-stress condition of each group.

IV. ANALYTICAL FRAMEWORK

A. Effective Fatigue Notch Factor from Surface Topography

Following the approach of Arola and Ramulu [15], the mean valley radius of curvature $\bar{\rho}$ is estimated from the RMS surface gradient Sdq:

$$\bar{\rho} = Sq / (2 \cdot Sdq^2) \qquad (1)$$

Substituting this into the Arola-Ramulu stress-concentration model gives the roughness-based notch factor:

$$K_{f,s} = 1 + n \cdot (Sq/\bar{\rho}) \cdot (1 + Sdr/100) \qquad (2)$$

which, after substituting for $\bar{\rho}$, reduces to the working form used in this study ($n = 0.5$, the notch-sensitivity coefficient appropriate to high-strength hardened steel under rotating bending [15]):

$$K_{f,s} = 1 + 2n \cdot Sdq^2 \cdot (1 + Sdr/100) \qquad (3)$$

where Sdq (rad) and Sdr (%) together describe both the sharpness of the valleys and the areal complexity of the texture. The resulting EFNF values are given in Table V.

TABLE V. CALCULATED EFNF BY GROUP

Group	Sq (µm)	Sdq (rad)	Sdr (%)	Kf,s
A	0.24	0.08	0.31	1.014
B	0.97	0.22	2.37	1.129
C	2.51	0.48	10.60	1.361

B. Residual Stress Influence Factor

Under fully reversed rotating bending the externally applied mean stress is zero, so any non-zero mean stress at the surface comes entirely from the residual stress σ_{RS}. Because the applied stress in rotating bending is uniaxial, the residual-stress mean-stress term can be used directly without a von Mises correction:

$$\sigma_{RS,mean} = \sigma_{RS} \qquad (4)$$

International Journal of Engineering Research & Technology (IJERT)
ISSN: 2278-0181
Vol. 14, Issue 09, RTMSE-2026

and, using a modified-Goodman form with the carburized ultimate strength Su = 1420 MPa for EN353, the residual stress influence factor is:

$$RSIF = 1 - \sigma_{RS,mean} / S_u \quad (5)$$

so RSIF > 1 for compressive σRS (beneficial) and RSIF < 1 for tensile σRS (detrimental). Table VI lists the resulting values, using the post-finishing surface stresses from Table IV.

TABLE VI. CALCULATED RSIF BY GROUP

Group	σRS (MPa)	Su (MPa)	RSIF
A	-380	1420	1.268
B	-395	1420	1.278
C	-360	1420	1.254

Fig. 5 shows how each factor moves across the practical range of roughness and residual stress covered by the three groups.

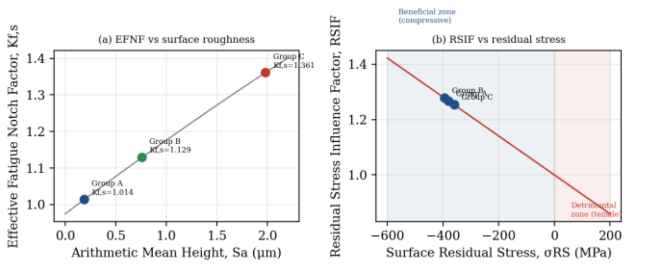

Fig. 5. (a) EFNF vs. Sa; (b) RSIF vs. surface residual stress. Markers show the measured values for Groups A-C.

C. Combined S-N Model

The two factors are brought together by scaling the applied bending stress amplitude into an effective amplitude before it is compared against a baseline S-N curve for a smooth, near-zero-residual-stress reference condition:

$$\sigma_{a,eff} = (\sigma_a \cdot K_{f,s}) / RSIF \quad (6)$$

$$\sigma_a = A \cdot N_f^{\,b} \quad (7)$$

with A = 1285 MPa and b = -0.094 obtained by least-squares regression of an electropolished reference data set (R^2 = 0.964). Predicted life Np follows by substituting σa,eff for σa in (7) and solving for Nf.

V. RESULTS AND DISCUSSION

A. Case Microstructure

Sectioned specimens showed the expected graded structure - a white martensitic case grading through a mixed martensitic-bainitic zone into a ferritic-pearlitic core. The effective case depth measured 0.82 - 0.97 mm across the batch, within the 0.8 - 1.0 mm target, with 12 - 18% retained austenite at the surface by XRD peak-intensity ratio - typical for this carburizing cycle. Surface hardness of 730 - 780 HV falling to a core of 320 - 380 HV (Fig. 2) confirms the case was formed as intended, so any differences in fatigue life between groups can reasonably be attributed to surface condition rather than to variation in the case itself.

B. Fatigue Life vs. Surface Roughness

Table VII collects the median fatigue life at each stress level for all three groups, and Fig. 6 plots the same data together with the model curves.

TABLE VII. MEDIAN FATIGUE LIFE NF (CYCLES), ROTATING BENDING, R = -1

σa (MPa)	Grp A	Grp B	Grp C
850	3.2×10^3	2.1×10^3	1.3×10^3
750	2.8×10^4	1.4×10^4	6.8×10^3
650	2.1×10^5	8.9×10^4	3.7×10^4
575	1.4×10^6	4.6×10^5	1.5×10^5
500	8.6×10^6	2.1×10^6	6.4×10^5
450	$>10^7$ (R/O)	7.8×10^6	2.3×10^6
420	$>10^7$ (R/O)	$>10^7$ (R/O)	8.9×10^6
400	-	$>10^7$ (R/O)	$>10^7$ (R/O)

R/O = run-out at 10^7 cycles.

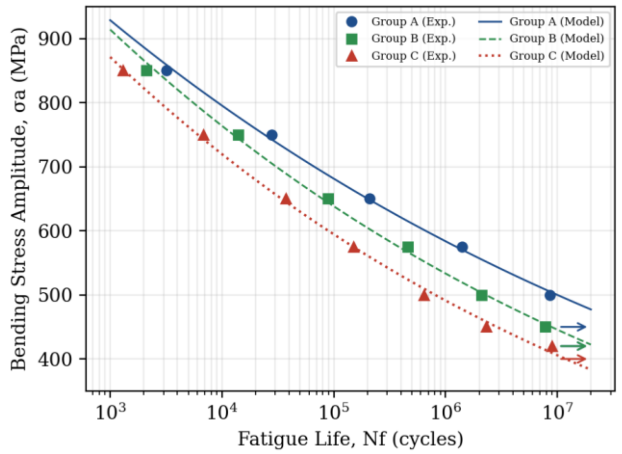

Fig. 6. Experimental S-N data and model predictions for Groups A-C. Arrows mark run-out specimens.

Life falls off steadily as the surface roughens, at every stress level tested. At σa = 650 MPa, for example, Group A reaches a median 2.1×10^5 cycles against 8.9×10^4 for Group B and 3.7×10^4 for Group C - roughly a 2.4-fold and 5.7-fold drop, respectively, for the rougher surfaces. The run-out (10^7-cycle) fatigue limit is far less sensitive to roughness than the finite-life region is: it drops from about 450 MPa for Group A to 420 MPa for Group B and roughly 400 MPa for Group C, a fall of only about 7% and 11%. That the fatigue limit holds up much better than the finite-life data is consistent with the compressive residual stress remaining largely intact at these lower amplitudes, so it continues to hold crack initiation back even as roughness increases.

The EFNF captures this mechanistically: rougher surfaces carry larger Sdq and Sdr, meaning deeper, more closely spaced valleys with sharper roots, which raises the local bending stress concentration at the surface. Because rotating bending drives the fluctuating tensile component that promotes Mode I crack initiation, these valleys become the preferred initiation sites. The negative skewness (Ssk) seen in Groups A and B points to a surface of deep valleys sitting below comparatively flat peaks - a shape that is particularly unfavourable under bending because it is exactly in those valleys that the local tensile stress is amplified and cracks tend to start.

International Journal of Engineering Research & Technology (IJERT)
ISSN: 2278-0181
Vol. 14, Issue 09, RTMSE-2026

C. Fatigue Life vs. Residual Stress

The compressive residual stresses of -360 to -395 MPa measured after finishing (Table IV) correspond to RSIF values of 1.25 - 1.28 - equivalent to a 25-28% increase in the bending stress amplitude a group can sustain for a given life, which is broadly in line with values reported elsewhere for carburized steels [22]. The depth profiles (Fig. 4) show the compressive peak (-450 to -500 MPa) sitting 0.05 - 0.10 mm below the surface, falling to zero near the case-core boundary and turning modestly tensile (+80 to +120 MPa) in the core. Since the maximum bending stress in rotating bending occurs right at the surface, it is exactly there that the compressive residual stress is most effective at reducing the mean tensile stress driving crack initiation and early growth.

One further pattern is worth noting: the fatigue lives of the three groups converge at the highest stress amplitude tested (σa = 850 MPa). This is consistent with residual stress relaxation - once the applied bending amplitude exceeds the local cyclic yield strength, the residual stress relaxes within the first few loading cycles and its RSIF benefit is largely lost, narrowing the gap between groups. At amplitudes below the fatigue limit, by contrast, the residual stress stays essentially unchanged, which agrees with the behaviour reported by Zhuang and Halford [18].

D. Model Validation

Table VIII compares predicted (Np) and experimental (Nf) fatigue lives at four stress levels per group, and Fig. 7 plots the same comparison as a parity chart.

TABLE VIII. PREDICTED VS. EXPERIMENTAL FATIGUE LIFE

Group	σa (MPa)	Nf (exp.)	Np (pred.)
A	750	2.8×10^4	3.1×10^4
A	650	2.1×10^5	2.3×10^5
A	575	1.4×10^6	1.6×10^6
A	500	8.6×10^6	9.2×10^6
B	750	1.4×10^4	1.5×10^4
B	650	8.9×10^4	9.7×10^4
B	575	4.6×10^5	5.1×10^5
B	500	2.1×10^6	2.3×10^6
C	750	6.8×10^3	7.8×10^3
C	650	3.7×10^4	4.4×10^4
C	575	1.5×10^5	1.8×10^5
C	500	6.4×10^5	7.8×10^5

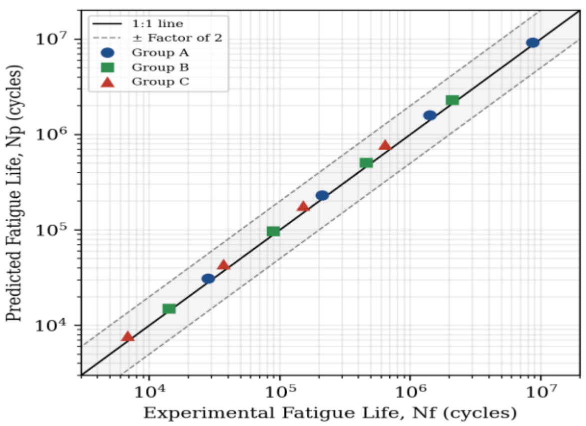

Fig. 7. Parity plot of predicted vs. experimental fatigue life for all groups; dashed lines mark the ±factor-of-two band.

The predicted-to-experimental ratio Np/Nf ranges from 1.07 to 1.22, i.e. the model is slightly conservative-leaning (over-predicts life a little) but comfortably inside the ±factor-of-two scatter band that is generally accepted for engineering fatigue-life work. Two effects likely explain the small systematic over-prediction: the EFNF formulation does not allow for partial crack closure that the local compressive stress field produces within surface valleys, which would otherwise trim the predicted stress concentration a little at low Kf,s; and the regression constants A and b carry some statistical uncertainty of their own, inherited from the finite size of the reference data set used to fit them. Neither materially detracts from the practical usefulness of the combined EFNF-RSIF approach for rotating bending fatigue assessment.

E. Fractography

The fracture patterns (summarised schematically in Fig. 8) track the roughness and residual-stress condition of each group closely. Group A specimens generally failed from one, or at most two or three, initiation sites at isolated grinding marks or subsurface inclusions, with clear concentric beach marks and a fast-fracture zone covering 20-30% of the cross-section - a pattern typical of rotating bending fatigue with a well-defined single dominant crack. Group B specimens showed several distributed initiation sites, visible striations under higher magnification, and a somewhat smaller fast-fracture zone (about 15-20%). Group C specimens were the most fragmented: initiation spread over a large part of the gauge circumference, cracks coalesced early, and the beach marks were shallow and widely spaced, consistent with rapid propagation. The circumferential lay left by turning puts the roughness valleys roughly perpendicular to the fluctuating bending stress, which is the worst possible orientation for stress concentration and helps explain why Group C initiates at so many sites at once.

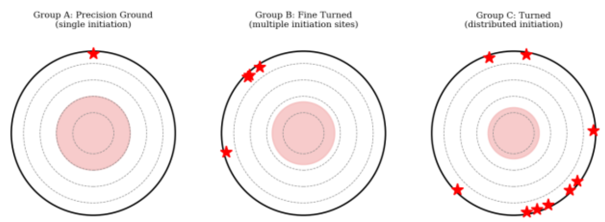

Fig. 8. Schematic fracture maps from optical microscopy. Stars = initiation sites; shaded zone = fast-fracture region.

VI. CONCLUSIONS

Rotating bending fatigue tests on case-carburized EN353 steel, combined with an EFNF-RSIF analytical framework, lead to the following conclusions.

1) Surface roughness has a substantial effect on rotating bending fatigue life: the EFNF rose from 1.014 (precision-ground) to 1.361 (conventionally turned), and fatigue life at intermediate stress amplitudes fell by up to 5.7-fold between these two conditions.

2) Compressive residual stresses of -360 to -395 MPa generated during carburizing and quenching gave RSIF values of 1.25 - 1.28, equal to a 25-28% increase in sustainable bending stress amplitude, by suppressing both crack initiation and early near-surface crack growth.

International Journal of Engineering Research & Technology (IJERT)
ISSN: 2278-0181
Vol. 14, Issue 09, RTMSE-2026

3) The combined EFNF-RSIF model reproduced the measured rotating bending fatigue lives within a factor of 1.07 - 1.22, well inside the ±factor-of-two band normally accepted in engineering fatigue assessment.

4) Fractography confirmed the mechanism: rougher surfaces promoted distributed circumferential crack initiation and earlier crack coalescence, while compressive residual stress confined initiation to isolated surface or subsurface defects.

5) Residual stress relaxation at high cyclic amplitudes reduced the RSIF benefit and narrowed the fatigue-life gap between groups at high stress; below the fatigue limit, residual stresses stayed essentially stable.

6) Routine measurement of EFNF and RSIF is worth building into manufacturing quality control for fatigue-critical case-hardened rotating components.

ACKNOWLEDGMENT

The authors thank the technical staff of the Materials Testing Laboratory, Department of Mechanical Engineering, Punjabi University, Patiala, for their help with specimen preparation, heat treatment and mechanical testing, and the Central Instrumentation Laboratory for access to the XRD and profilometry equipment used in this work. This research received no specific grant from any funding agency. The authors declare no conflict of interest.

REFERENCES

[1] D. F. Socie and G. B. Marquis, Multiaxial Fatigue. Warrendale, PA: SAE International, 2000.

[2] ASM International, ASM Handbook Volume 4: Heat Treating. Materials Park, OH: ASM International, 2002.

[3] G. Parrish, Carburizing: Microstructures and Properties. Materials Park, OH: ASM International, 1999.

[4] D. Arola and C. L. Williams, “Estimating the fatigue stress concentration factor of machined surfaces,” Int. J. Fatigue, vol. 24, no. 9, pp. 923-930, 2002.

[5] D. Novovic, R. C. Dewes, D. K. Aspinwall, W. Voice, and P. Bowen, “The effect of machined topography and integrity on fatigue life,” Int. J. Mach. Tools Manuf., vol. 44, no. 2-3, pp. 125-134, 2004.

[6] P. J. Withers and H. K. D. H. Bhadeshia, “Residual stress: Part 1 — Measurement techniques,” Mater. Sci. Technol., vol. 17, no. 4, pp. 355-365, 2001.

[7] S. Suresh, Fatigue of Materials. Cambridge, UK: Cambridge Univ. Press, 1998.

[8] A. Javidi, U. Rieger, and W. Eichlseder, “The effect of machining on the surface integrity and fatigue life,” Int. J. Fatigue, vol. 30, no. 10-11, pp. 2050-2055, 2008.

[9] G. Parrish, The Influence of Microstructure on the Properties of Case-Carburised Components. Metals Park, OH: ASM International, 1980.

[10] G. Krauss, “Martensite in steel: strength and structure,” Mater. Sci. Eng. A, vol. 273-275, pp. 40-57, 1999.

[11] A. Bensely, A. Prabhakaran, D. Mohan Lal, and G. Nagarajan, “Enhancing the wear resistance of case carburized steel (En 353) by cryogenic treatment,” Cryogenics, vol. 45, no. 12, pp. 747-754, 2006.

[12] O. Asi, A. Ç. Can, J. Pineault, and M. Belassel, “The effect of high temperature gas carburizing on bending fatigue strength of SAE 8620 steel,” Mater. Des., vol. 30, no. 5, pp. 1792-1797, 2009.

[13] H. Neuber, “Theory of stress concentration for shear-strained prismatic bodies with arbitrary nonlinear stress-strain law,” J. Appl. Mech., vol. 28, no. 4, pp. 544-550, 1961.

[14] Y. Murakami and M. Endo, “Effects of defects, inclusions and inhomogeneities on fatigue strength,” Int. J. Fatigue, vol. 16, no. 3, pp. 163-182, 1994.

[15] D. Arola and M. Ramulu, “An examination of the effects of surface texture on the strength of fiber reinforced plastics,” J. Compos. Mater., vol. 33, no. 2, pp. 102-123, 1999.

[16] P. S. Prevéy, “The effect of cold work on the thermal stability of residual compression in surface enhanced IN718,” in Proc. 20th ASM Heat Treating Conf., 2000, pp. 426-434.

[17] J. A. Bannantine, J. J. Comer, and J. L. Handrock, Fundamentals of Metal Fatigue Analysis. Englewood Cliffs, NJ: Prentice Hall, 1989.

[18] W. Z. Zhuang and G. R. Halford, “Investigation of residual stress relaxation under cyclic load,” Int. J. Fatigue, vol. 23, suppl. 1, pp. S31-S37, 2001.

[19] M. A. S. Torres and H. J. C. Voorwald, “An evaluation of shot peening, residual stress and stress relaxation on the fatigue life of AISI 4340 steel,” Int. J. Fatigue, vol. 24, no. 8, pp. 877-886, 2002.

[20] H. Kumar and S. Bhowmick, “Effect of case depth on the fatigue behaviour of EN353 steel,” J. Mater. Process. Technol., vol. 255, pp. 23-31, 2018.

[21] G. Singh and O. P. Pandey, “Short and long duration cryogenic treatment of EN353 steel: Effect on mechanical properties, residual stresses and microstructure,” Mater. Chem. Phys., vol. 229, pp. 1-15, 2019.

[22] K. H. Lang and D. Löhe, “Influence of warm peening on the fatigue behaviour of differently heat-treated steel specimens,” in Proc. 8th Int. Conf. Shot Peening, 2002, pp. 16-20.